ACS Catalysis

pubs.acs.org/acscatalysis

Research Article

Surfactant Perturbation of Cation Interactions at the Electrode–Electrolyte Interface in Carbon Dioxide Reduction

Soumyodip Banerjee, Zhuo-Qun Zhang, Anthony Shoji Hall, and V. Sara Thoi*

Cite This: *ACS Catal.* 2020, 10, 9907–9914

Read Online

ACCESS | Metrics & More | Article Recommendations | Supporting Information

ABSTRACT: Interfacial properties at the boundary between the electrode and electrolyte have important effects on the surface reactivity in electrocatalysis. Ionic additives and electrolyte ions can serve as promoters for specific reaction pathways. The judicious addition of these charged species thus represents a rich chemical strategy for tuning the electrode–electrolyte interface to achieve high product selectivity and catalytic activity. We have previously shown that trace amounts of surfactant can efficiently suppress the hydrogen evolution reaction (HER) and promote the carbon dioxide reduction (CO_2RR) toward CO and $HCOO^-$ on a polycrystalline Cu foil working electrode. The major focus of herein study is to identify the impact of a model surfactant, cetyltrimethylammonium bromide (CTAB), on the double-layer structure in the presence of different alkali metal cations during electrocatalytic CO_2RR. We postulated that the alkali cations and the positively charged surfactant headgroup will compete for a position at the negatively biased Cu electrode, leading to potentially synergistic effects on the catalytic performance. Indeed, it was observed that the positively charged trimethylammonium surfactant molecules effectively displace the alkali cations and suppress HER. However, the CO_2RR activity and selectivity are nearly independent with respect to the identity of the alkali cations (Li^+, Na^+, and K^+) in the presence of CTAB. Cesium cations defy this trend, where high $HCOO^-$ activity is observed. A molecular model of the double layer is proposed where CTAB molecules are competing for a position at the outer Helmholtz plane (OHP), resulting in only a small concentration of electrolyte cation at the electrode surface in the presence of CTAB. Furthermore, we postulate that the decrease in C_2H_4 activity is due to interfacial hydrophobicity caused by surfactant accumulation. We expect that these fundamental understandings will lead to advanced strategies for designing efficient organic additive to modulate the double-layer structure and optimize for selective small-molecule activation.

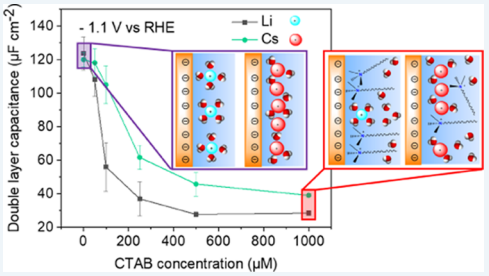

KEYWORDS: *electrochemical impedance spectroscopy, electrocatalysis, electrode–electrolyte interface, hydrogen evolution, carbon conversion, ATR-SEIRAS*

INTRODUCTION

Electrochemical conversion of CO_2 to high-energy-density fuels and other important chemicals has the potential to meet the increasing global demand for new energy sources. Intense research efforts have been focused on developing novel catalytic materials and understanding the influence of structural,[1−4] compositional,[5−13] and crystallographic properties[14,15] of metallic catalysts on the carbon dioxide reduction reaction (CO_2RR). However, recent studies have shown that experimental parameters such as temperature,[16] partial pressure of CO_2,[17] and other electrolyte conditions play critical roles in dictating both CO_2RR selectivity and activity. For instance, trace metal impurity associated with bicarbonate and carbonate salts,[18,19] Ag/AgCl reference electrodes,[20] and even trace gaseous impurity[21] in reagent gas stream has been witnessed to dramatically steer the hydrogen evolution reaction (HER) and CO_2RR selectivity. The use of chelating agents[18] and different halide anions[22] can also drive CO_2RR selectivity by modulating the trace impurity ion concentration and atop CO coverage,[23] respectively. These findings demonstrate that the chemical interactions at the electrode–electrolyte interface can heavily impact surface reactivity and modify the reaction mechanism.[24−26] Also, tuning of the electrolyte pH has been shown to alter the reaction kinetics and therefore CO and $HCOO^-$ selectivity.[27] Taking advantage of these interfacial properties offer an additional chemical handle toward enhancing catalytic performance.

Of particular interest is developing novel strategies to suppress the hydrogen evolution reaction (HER). The influence of electrolyte cations is already recognized in interfacial electrochemistry.[28] The smaller hydrated cations such as Li^+ was shown to stabilize the hydroxide species adsorbed on Pt through noncovalent interaction. The non-

Received: May 30, 2020
Revised: August 1, 2020
Published: August 7, 2020

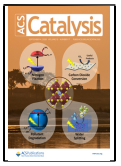

covalent interaction and site blocking was proposed to be the reason behind superior oxygen reduction (ORR), methanol oxidation, and hydrogen oxidation (HOR) performance of Pt in presence of larger cation under alkaline condition.[29] Also, the larger cations were previously reported to affect the C_2 product selectivity in electrocatalytic CO_2RR on Cu foil.[30] The size of the hydrated cations can further enhance CO_2RR; for instance, Cs^+ ions can more readily undergo hydrolysis at the biased electrode and help maintain an interfacial pH very close to neutral value.[31−33] The near-neutral local pH ensures a high local CO_2 concentration, which improves both the catalytic activity and selectivity.[34] The electrolyte cations can also modulate the electric field at the interface, which has been proposed to stabilize certain surface-bound intermediates.[31,35]

Besides inorganic cations, organic cations[36,37] and ionic liquids[38−41] have attracted attention due to their unique ability to suppress parasitic processes during electrocatalysis. Recently, we demonstrated that trimethylammonium surfactants lead to dramatic hydrogen evolution reaction (HER) suppression and enhanced CO_2RR selectivity toward CO and $HCOO^-$.[25] Based on vibrational stark shift spectroscopy, electrochemical impedance spectroscopy (EIS), and modeling, we proposed that the trimethylammonium headgroup accumulates and aligns along the electrode surface.[25,42] The ease of surface accumulation was attributed to the ability of the alkyl tail to form favorable hydrophobic interactions. Moreover, our hypothesized cetyltrimethylammonium bromide (CTAB)-mediated HER suppression model was further solidified in another recent spectroscopic study.[43] A reorganization and displacement of interfacial water molecules observed in the presence of CTAB in the double layer. Herein, we focus on the interplay between different alkali cations and cetyltrimethylammonium bromide (CTAB) and their collective impact on CO_2RR selectivity. Despite the high solution concentration of the alkali cations compared to the surfactant, we discovered that the trimethylammonium headgroup effectively displaces most of the alkali cations tested at the biased interface and suppresses HER. However, cetyltrimethylammonium bromide (CTAB) has been observed to generate exceptionally high amount of $HCOO^-$ in Cs^+-containing electrolytes. In addition, C−C coupled products were inhibited in the presence of CTAB. Using a combination of surface-enhanced infrared absorption spectroscopy (SEIRAS) and electrochemistry, we developed a chemical model to explain these unusual catalytic trends. This fundamental investigation offers new chemical strategies to modulate the electrode−electrolyte interface, with the eventual goal of designing efficient and inexpensive catalytic systems for carbon dioxide conversion.

EXPERIMENTAL SECTION

Materials and Instrumentation. Cu foil (99.999%, Alfa Aesar), Ag foil (99.9%, Alfa Aesar), lithium carbonate (99.997%, Sigma-Aldrich), sodium carbonate (99.999%, Sigma-Aldrich), potassium carbonate (99.995%, Sigma-Aldrich), cesium carbonate (99.995%, Sigma-Aldrich), tetramethylammonium bromide (TMAB) (98.0%, Acros Organics), (1-octyl)trimethylammonium bromide (≥98%, Sigma-Aldrich), (1-decyl)trimethylammonium bromide (98%, Alfa Aeser), dodecyltrimethylammonium bromide (99%, Acros Organics), cetyltrimethylammonium bromide(>99%, Acros Organics), carbon dioxide (≥99.9%, Airgas), and dimethyl sulfoxide (≥99.9%, Fisher Scientific) were used in our experiments. A Ag/AgCl (3 M NaCl) reference electrode (BASI) and a graphite counter electrode (99.9995%, Alfa Aesar) were utilized in the electrochemical experiments.

The controlled potential electrolysis was carried out in a gas-tight two-compartment electrochemical cell purchased from Adams and Chittenden Scientific Glass, where the cathodic and anodic chambers (70 mL each side) are separated by a glass frit. The headspace of the cathodic chamber was connected to an Agilent Micro GC 490 equipped with PoraPlot (U) column and a Molsieve 5A column to facilitate the analysis of gaseous products after electrolysis. The liquid products were analyzed with a Bruker Avance 400 MHz NMR spectrometer. All electrochemical experiments were conducted on an Ivium n-STAT multichannel electrochemical analyzer, and all electrochemical data were analyzed on IviumSoft software. A Mettler Toledo Five Easy Plus pH meter (FEP20) was used to determine the pH of the bulk electrolyte.

Electrode Preparation. For electrochemical experiments, the metal foil (Cu or Ag) was cut into square pieces and polished with 800 grit abrasive paper for at least 5 min until a mirror finish was achieved. The foil was sonicated in Milli-Q water for 5 min and dried under N_2 flow. Then, the foil was wrapped with Ag wire and the edges of the foil and the exposed wire were masked using polyimide tape to expose only 1 cm^2 area of the electrode to the electrolyte.

Controlled Potential Electrolysis. Typically, 0.05 M M_2CO_3 (M = Li, Na, K, Cs) solutions were used as electrolytes in electrochemical experiments. The electrolyte solutions were prepared by dissolving high-purity metal carbonate salts in Milli-Q water and were used without any further purification. The metal (Cu or Ag) foil working electrode and the Ag/AgCl reference electrode were placed in the cathodic chamber, and the graphite rod counter electrode was placed in the other chamber. Both chambers were filled with 40 mL of electrolyte solution, and CO_2 gas was purged through the solution for 20 min to ensure saturation. For CO_2, the pH was 6.8 after saturation and the bulk electrolyte pH was maintained throughout the electrolysis. After 20 min of continuous CO_2 purging, the purging needles were removed from the solution and a concentrated surfactant solution was introduced to electrolytes to maintain a final concentration at 1 mM. All electrochemical experiments have been performed at this surfactant concentration unless mentioned otherwise. Carbon monoxide reduction (CORR) was also conducted in an analogous fashion, though CO saturation does not impact the bulk pH.

Before applying a potential, the solution resistance was measured by electrochemical impedance spectroscopy. The real component of the Nyquist plot at 10^4 Hz was used as the solution resistance. Typically, 85% of the solution resistance was compensated automatically by the software. The electrolysis was carried out for 1 h at −1.1 V vs reversible hydrogen electrode (RHE) (after 85% Ohmic compensation), and all of the experiments were repeated three times to establish error bars. The potential values were reported after compensating the remaining 15% Ohmic drop manually post electrolysis. The actual average electrolysis potential is −1.05 ± 0.01 V vs RHE.

RESULTS AND DISCUSSION

To uncover the interplay between alkali cations and trimethylammonium surfactant at the electrode surface, a series of controlled potential electrolysis was performed with a

https://dx.doi.org/10.1021/acscatal.0c02387
ACS Catal. 2020, 10, 9907−9914

planar Cu foil working electrode in 0.05 M M_2CO_3 electrolytes, where M = Li^+, Na^+, K^+, and Cs^+. An applied potential of −1.05 V vs RHE was chosen to not only probe the electrolyte−surfactant interactions but to also observe the impact of the CTAB toward hydrocarbon selectivity. As shown in Figure 1, the HER activity and selectivity are influenced by

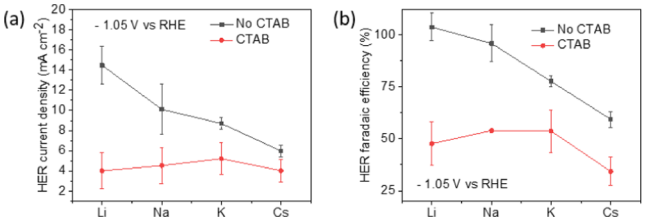

Figure 1. (a) HER current density and (b) Faradaic efficiency for electrolysis carried out with Cu foil in the absence (black) and in the presence (red) of CTAB in CO_2-saturated 0.05 M M_2CO_3 (M = Li, Na, K, Cs) at −1.05 V vs RHE.

the identity of the electrolyte cation. Consistent with previous reports,[44] the HER current density is suppressed from Li^+ to Cs^+ in CTAB-free electrolyte at −1.05 V vs RHE (Figure 1a,b, black squares). The addition of CTAB further diminishes the HER current density and Faradaic efficiency, though both the absolute activity and selectivity appear to be independent of the alkali cation (Figure 1a,b, red circles). A similar HER trend is observed when electrolysis is carried out with a mechanically polished Ag foil at −1.05 V vs RHE (Figure S1). These results suggest that the HER suppression effects of the surfactant dominate over the influence of the different alkali cations.

It has been observed that the identity of the alkali cation plays a major role in the formation of high-order carbon products.[31,32,44] In the absence of CTAB, CO_2RR products show the expected cation dependent activity and selectivity trend (Figure 2), which is manifested by an increase of C_2H_4 current density and efficiency from Li^+ to Cs^+. However, the alkali cation influence on C−C bond formation is weakened in CTAB-containing electrolytes. In the presence of CTAB, CO, CH_4, and C_2H_4, activity and selectivity are similar in all four electrolytes (Figure 2). Likewise, $HCOO^-$ activity is similar in Li^+-, Na^+-, and K^+-containing electrolytes in the presence of CTAB, but an unexpected enhancement in $HCOO^-$ activity and selectivity are observed in the Cs^+-containing electrolyte.

The mixed influence of CTAB on CO_2RR in different electrolytes requires a closer examination of the electrode−electrolyte interface. Evaluating the two extremes, a series of controlled potential electrolysis was performed in Li^+- and Cs^+-containing electrolytes with a different bulk concentration of CTAB at −1.05 V. In the Li^+ electrolyte, the HER current density declines sharply (Figure 3a, black squares) even in the presence of 50 μm CTAB, while the decrease in the HER activity is more gradual in Cs^+-containing electrolytes (Figure 3a, green circles). The effect of CTAB on different CO_2RR products is also dependent on the electrolyte cations. The introduction of CTAB enhances CO and $HCOO^-$ activity in both Li^+- and Cs^+-containing electrolytes (Figure 3b,c). A small increase is observed for C_2H_4 activity in the Li^+-containing electrolyte (Figure 3b). In contrast, C_2H_4 current density significantly drops when CTAB is introduced to the Cs^+ electrolyte (Figure 3c). These findings show that the presence of CTAB leads to an enhancement in $HCOO^-$ but disfavors C−C bond formation particularly in the presence of Cs^+.

To develop a better understanding of the electrode local environment, infrared spectra were collected on a Cu-coated Si prism in attenuated total reflectance surface-enhanced infrared absorption spectroscopy (ATR-SEIRAS) configuration (see the Supporting Information) in Li^+- and Cs^+-containing electrolytes in the presence and absence of CTAB. A constant cathodic potential at −1.1 V vs RHE was applied for 7 min to monitor the temporal evolution of the double-layer environment, where the population of surface-adsorbed species (H_2O, CO, and CTA^+) was analyzed by the integration of the corresponding IR band. A broad band was observed in both Li^+- and Cs^+-containing electrolytes in the absence of CTAB within the frequency range of 3750−3010 cm^{-1} (Figure 4a−d), which corresponds to the O−H stretching mode (ν-OH) of interfacial water. The integrated area for the ν-OH band increases over time (Figure 4e,f, black squares), indicating interfacial water molecules may reorient with protons tilted toward the electrode and/or an increase of interfacial concentration caused by an electro-wetting effect upon an applied cathodic bias.[45] In the presence of CTAB, the intensity

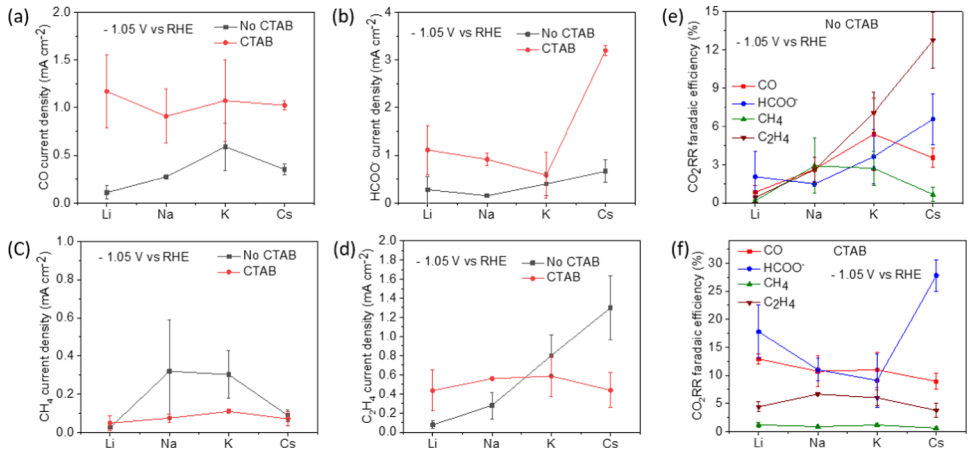

Figure 2. (a) CO, (b) $HCOO^-$, (c) CH_4, and (d) C_2H_4 current density in CO_2-saturated 0.05 M M_2CO_3 (M = Li, Na, K, Cs) in the presence and absence of CTAB. CO_2RR Faradaic efficiency data for electrolysis carried out (e) in the presence and (f) absence of CTAB in four different electrolytes at −1.05 V vs RHE.

https://dx.doi.org/10.1021/acscatal.0c02387
ACS Catal. 2020, 10, 9907−9914

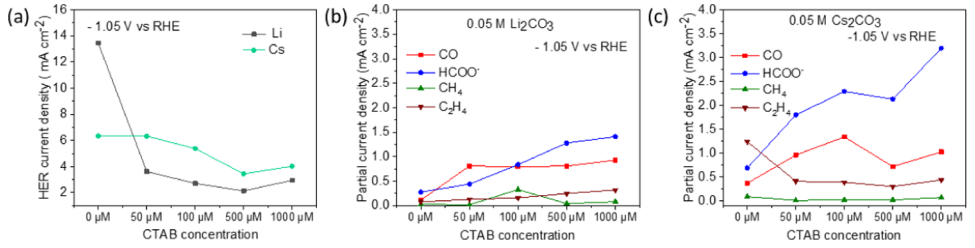

Figure 3. (a) HER current density in the absence and presence of different concentrations of CTAB in Li^+- (black squares) and Cs^+- (green circles) containing electrolytes, and CO_2RR current density in the absence and presence of different concentrations of CTAB in (b) Li^+- and (c) Cs^+-containing electrolytes at −1.05 V vs RHE.

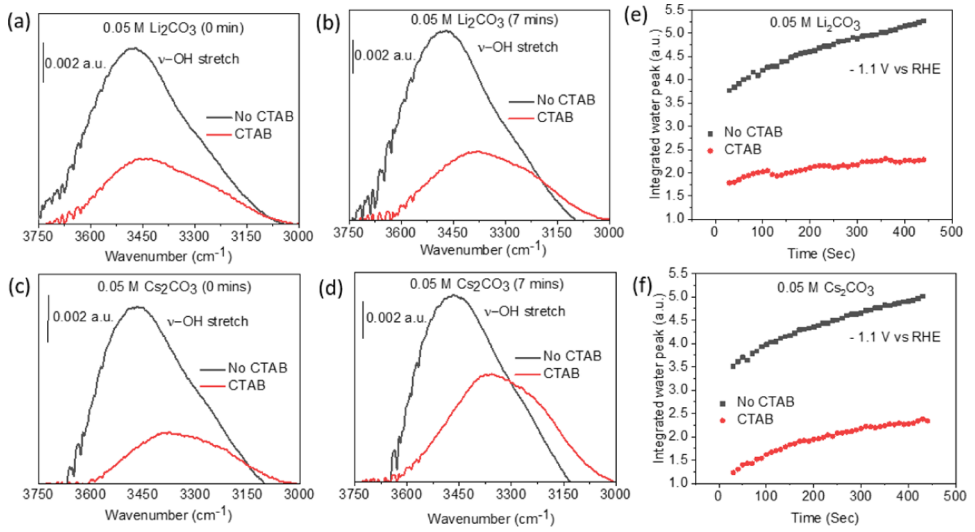

Figure 4. Interfacial water absorption (ν-OH) band at a frequency range of ∼3750 to 3010 cm^{-1} in the absence (black) and in the presence of 1 mM CTAB (red) in CO_2-saturated 0.05 M Li_2CO_3 at (a) 0 min and (b) 7 min time point of electrolysis at −1.1 V vs RHE, in CO_2-saturated 0.05 M Cs_2CO_3 for (c) 0 min and (d) 7 min time point of electrolysis at −1.1 V vs RHE. The temporal evolution of the integrated water band in the absence (black squares) and in the presence (red circles) of CTAB in (e) Li^+- and (f) Cs^+-containing electrolytes.

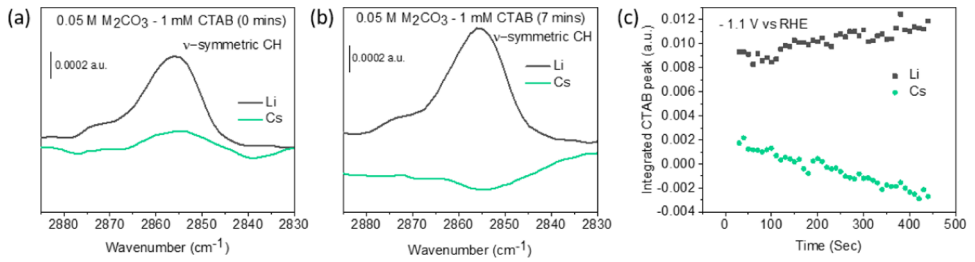

Figure 5. Symmetric C−H stretching band of CTAB at a frequency range of ∼2875 to 2839 cm^{-1} in the presence of 1 mM CTAB in Li^+- (black) and Cs^+- (green) containing electrolytes at (a) 0 and (b) 7 min time point of electrolysis at −1.1 V vs RHE, and (c) temporal evolution of the integrated C−H stretching band at −1.1 V vs RHE in Li^+- (black squares) and Cs^+- (green circles) containing electrolytes.

of the ν-OH band also slowly increases, though the band amplitude is much lower in both electrolytes (Figure 4a−d, red traces), suggesting that the interfacial water molecules are displaced more readily at the biased electrode upon the introduction of CTAB.[43] The displacement of interfacial water by CTA^+ also decreases the concentration of protic sources, which is likely responsible for the enhanced HER suppression. We have previously observed that the addition of CTA^+ to the electrolyte leads to decreased interfacial concentration of water and bicarbonate.[43] We note that the higher CTAB concentration in the present study may lead to micelle formation and result in lower freely diffusing CTA^+ cations at the electrode surface compared to our prior work.[43] In addition to the water band, atop CO (defined as a CO bound to a single Cu atom) was observed at a frequency region ∼2070 cm^{-1} (Figure S2). In both electrolytes, the integrated band intensity of atop CO dropped sharply within the first 300 s, though higher interfacial CO coverage was maintained in Li-based electrolytes in all cases.

Furthermore, we tracked an absorbance peak corresponding to the symmetric C−H stretching region (2875−2839 cm^{-1}) of the CTA^+ to identify the impact of the electrolyte cation toward the surfactant cation accumulation at the outer Helmholtz plane (OHP). In Li^+-containing electrolyte, the strong upward C−H stretching band (Figure 5a, black trace) indicates that the surfactant molecule strongly displaces hydrated Li^+ ions under cathodic potential at all time points. On the other hand, a weak upward C−H vibration band

https://dx.doi.org/10.1021/acscatal.0c02387
ACS Catal. 2020, 10, 9907−9914

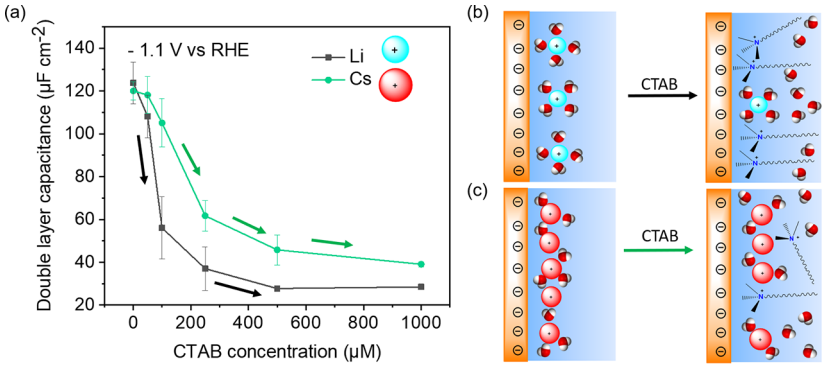

Figure 6. (a) Double-layer capacitance at −1.1 V vs RHE in the presence of different amount of CTAB in CO_2-saturated 0.05 M Li_2CO_3 (black squares) and Cs_2CO_3 (green circles), (b) proposed model for interfacial CTA^+ accumulation in Cs^+-containing electrolytes, and (c) proposed model for interfacial CTA^+ accumulation in Li^+-containing electrolytes.

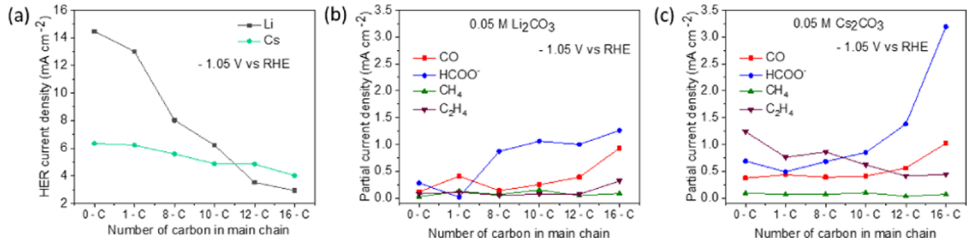

Figure 7. (a) HER current density at −1.05 V vs RHE in the absence and the presence of 1 mM surfactant comprising different number of carbon in a long chain in Li^+- (black squares) and Cs^+- (green circles) containing electrolytes, and CO_2RR partial current density at −1.05 V vs RHE in the absence and the presence of 1 mM surfactant comprising different number of carbon in a long chain in (b) Li^+- and (c) Cs^+-containing electrolytes.

(Figure 5a, green trace) is initially observed in Cs^+-containing electrolytes, but the intensity decreases over time (Figure 5b, green trace). The downward slope of the integrated C−H band with time (Figure 5c, green circles) suggests that although CTAB initially displaces hydrated Cs^+, an equilibrium is established over a short period of time where hydrated Cs^+ ions coexist with CTA^+ at the interface. The accumulation of hydrated Cs^+ is also observed by a qualitative comparison of the slope of the integrated water band as a function of time between Li^+- and Cs^+-containing electrolytes. In the presence of CTAB and Cs^+, the rate of interfacial water accumulation is higher than in the case of the Li^+ electrolyte (Figure S3). Along with the enhancement of C_2H_4 production, the larger cations have been previously recognized to enhance the rate of $HCOO^-$ production on Cu single-crystal electrodes in the absence of any additives.[31] Cation-assisted $HCOO^-$ enhancement has also been evidenced in our electrolyte-only controlled potential electrolysis experiments (Figure 2b,e). Taken together, we postulate that the combined field effects of Cs^+ and the hydrophobicity of CTA^+ are likely the reason for the unusually high $HCOO^-$ production in the presence of both cations.

We have previously demonstrated that electrochemical impedance spectroscopy measurements can be useful for tracking the evolution of double layer under electrocatalytic conditions.[25] Again drawing attention to the two extreme sizes for clarity, the double-layer capacitances are almost identical for Li^+ and Cs^+ electrolytes in the absence of CTAB at the cathodic potential of −1.1 V (Figure 6). Upon gradual addition of CTAB, the accumulation of the alkyl surfactant at the interface leads to a drop in the double-layer capacitance (C_{dl}) owing to its lower dielectric constant compared to water. However, the decline in C_{dl} is notably less steep in the case of Cs^+, with the final C_{dl} at 1000 μM CTAB higher than that of the Li^+ electrolyte. We note that similar trends are observed for all four electrolytes (Figures S4 and S5). These results provide further evidence that hydrated Cs^+ can more easily displace CTAB than hydrated Li^+. Owing to their more diffuse ionic charge, larger cations may easily liberate their solvation shell,[28] thus cations such as Cs^+ are more likely able to displace CTA^+ at the surface. In a few earlier studies,[31,46,47] the driving force of the alkali cation to accumulate at the Outer Helmholtz Plane (OHP) has been reported to increase with cation size. Their density-functional theory (DFT) calculations suggest that hydrated Cs^+ cations can form the most compact layer at the electrode−electrolyte interface, followed by K^+, Na^+, and Li^+. The C_{dl} trends borne out of our EIS study similarly imply that there are more Cs^+ ions at the interface compared to the other alkali cations at 1000 μM CTAB (Figure S5). The comparable CO_2RR and HER trends for Li^+, Na^+, and K^+ also corroborate with the hypothesis that CTAB molecules dominate at the electrode surface. It is only in the case of the Cs^+ electrolyte where differences in CO_2RR activity and selectivity are observed. As noted above, CTA^+ can form micellar assemblies above the critical micelle concentration of 1 mM,[48−50] which will impact the availability of freely diffusing CTA^+ cations at the electrode surface. We also note that surface reconstruction is not expected under these conditions.[25] Future investigations are focused on characterizing the hierarchal structures of CTAB at the electrode−electrolyte interface and examining their effects on cation accumulation.

To understand the product selectivity in the presence of CTA^+ and Cs^+ cations, controlled potential electrolysis was conducted in Li^+- and Cs^+-based electrolytes in the presence of trimethylammonium surfactants with different alkyl chains. Notably, the symmetric tetramethylammonium bromide

https://dx.doi.org/10.1021/acscatal.0c02387
ACS Catal. 2020, 10, 9907−9914

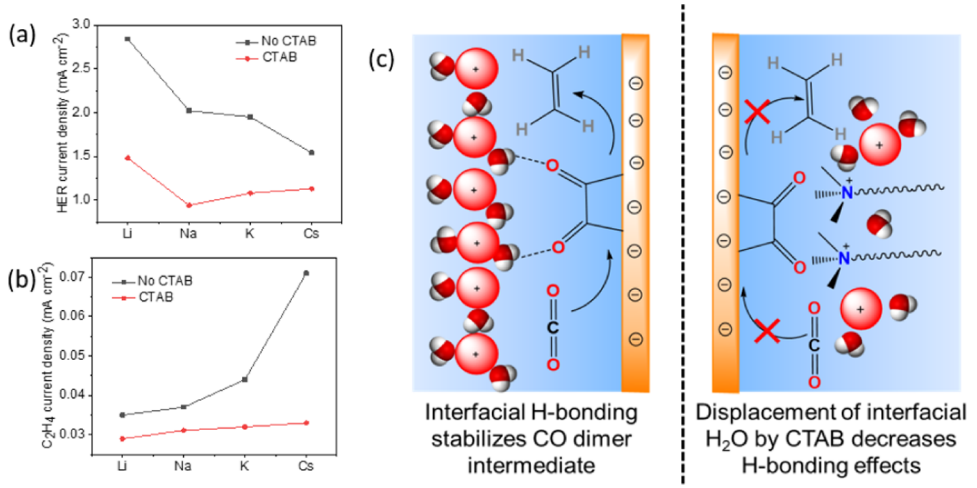

Figure 8. (a) HER, (b) C_2H_4 current density for CORR carried out in 0.05 M M_2CO_3 (M = Li, Na, K, Cs) at −0.75 V vs RHE in the absence and presence of 1 mM CTAB under a CO atmosphere, and (c) our proposed mechanism for the inhibition of C−C coupling in the presence of CTAB.

(TMAB) does not impact the HER and CO_2RR activity compared to the additive-free Li^+ and Cs^+ electrolytes (Figure 7a−c). This observation suggests that the long-chain alkyl groups play an intimate role in HER suppression. Increasing the chain length leads to greater HER suppression and enhanced CO and $HCOO^-$ activity for both electrolytes (Figure 7). In the Li^+ electrolyte, the C_2H_4 activity is relatively unchanged (Figure 7b), while a general decrease in C_2H_4 activity is observed in Cs^+-containing electrolytes in the presence of longer-chain surfactants (Figure 7c). The lack of enhancement and even decrease in C_2H_4 production in the presence of CTAB is consistent with a previous investigation in which tetraalkylammonium salts were used as electrolytes (in the absence of alkali cations). It was suggested that hydrophobic tetrabutylammonium cations hinder the CO dimerization pathway to C_2H_4 by disrupting the interfacial hydrogen bonding and impeding diffusion of local proton sources.[51] Given the hydrophobicity of the CTA^+ ion, we postulated a similar effect is at play in our system.

To examine the validity of the proposed C_2H_4 inhibition pathway, a series of carbon monoxide reduction (CORR) experiments were performed at −0.75 V vs RHE in different electrolytes in the presence of CTAB. The HER suppression (Figure 8a) is observed in the presence of CTAB in all four alkali cation electrolytes, and the overall product selectivity trends are very similar to those found in CO_2RR experiments. The only major CORR product is C_2H_4 under all circumstances. In the absence of CTAB, an increase of C_2H_4 activity (Figure 8b, black squares) is observed from Li^+ to Cs^+, which is consistent with previous reports.[52] In CTAB-containing electrolytes, the C_2H_4 activity is lower than the electrolyte-only situation (Figure 8b, red circles). The data supports that the hypothesis that interfacial hydrophobicity originated by the alkylammonium cation inhibits C−C bond formation pathway (Figure 8c).[51]

CONCLUSIONS

In summary, we have elucidated the interplay between alkali metal cations and trimethylammonium surfactant at the double-layer structure and their combined impact toward electrochemical CO_2RR. Our catalysis results indicate that the introduction of CTAB in Li^+-, Na^+-, and K^+-containing electrolytes leads to almost similar CO and $HCOO^-$ enhancement. In contrast, CTAB-containing Cs^+ electrolytes exhibit exceptionally high $HCOO^-$ activity and selectivity. We hypothesize that hydrated Li^+, Na^+, and K^+ can be relatively easy to be displaced by CTA^+ under catalytic conditions, while Cs^+ ions form a more compact layer that can compete with CTAB at the interface. We postulated that the significant Cs^+ concentration at OHP contributes to the high $HCOO^-$ activity and selectivity. Our proposed model is validated by extensive EIS experiments, in situ infrared spectroscopy, and CORR evaluation, which are consistent with previously reported DFT calculations and spectroscopic investigations. The decrease in hydrocarbon activity after the introduction of CTAB is likely due to the inhibition of interfacial hydrogen bonding at the electrode−electrolyte interface. We expect that these fundamental investigations will facilitate the design of novel additives for improved catalytic performance.

ASSOCIATED CONTENT

Supporting Information

The Supporting Information is available free of charge at https://pubs.acs.org/doi/10.1021/acscatal.0c02387.

Experimental details, spectroscopic data for CO adsorption, Nyquist plot, and simulations (PDF)

AUTHOR INFORMATION

Corresponding Author

V. Sara Thoi − *Department of Chemistry and Department of Materials Science and Engineering, Johns Hopkins University, Baltimore, Maryland 21218, United States;* orcid.org/0000-0003-0896-4077; Email: sarathoi@jhu.edu

Authors

Soumyodip Banerjee − *Department of Chemistry, Johns Hopkins University, Baltimore, Maryland 21218, United States*

Zhuo-Qun Zhang − *Department of Materials Science and Engineering, Johns Hopkins University, Baltimore, Maryland 21218, United States*

Anthony Shoji Hall − *Department of Materials Science and Engineering, Johns Hopkins University, Baltimore, Maryland 21218, United States;* orcid.org/0000-0003-4134-4160

Complete contact information is available at: https://pubs.acs.org/10.1021/acscatal.0c02387

https://dx.doi.org/10.1021/acscatal.0c02387
ACS Catal. 2020, 10, 9907−9914

Notes

The authors declare no competing financial interest.

■ ACKNOWLEDGMENTS

S.B. and V.S.T. thank the Department of Chemistry and Johns Hopkins University for instrumentation support, graduate student support, and start-up funding. A.S.H. acknowledges financial support from the National Science Foundation under award no. CHE-1764310. We also acknowledge the assistance of Dr. Marina A. Solomos, Eric Thompson, and Prof. Thomas Kempa for their assistance in metal evaporation.

■ REFERENCES

(1) Han, X.; Wang, M.; Le, M. L.; Bedford, N. M.; Woehl, T. J.; Thoi, V. S. Effects of Substrate Porosity in Carbon Aerogel Supported Copper for Electrocatalytic Carbon Dioxide Reduction. *Electrochim. Acta* **2019**, *297*, 545−552.

(2) Huan, T. N.; Simon, P.; Rousse, G.; Génois, I.; Artero, V.; Fontecave, M. Porous Dendritic Copper: An Electrocatalyst for Highly Selective CO2 Reduction to Formate in Water/Ionic Liquid Electrolyte. *Chem. Sci.* **2017**, *8*, 742−747.

(3) Kim, H.; Park, H. S.; Hwang, Y. J.; Min, B. K. Surface-Morphology-Dependent Electrolyte Effects on Gold-Catalyzed Electrochemical CO2 Reduction. *J. Phys. Chem. C* **2017**, *121*, 22637−22643.

(4) Hall, S. A.; Yoon, Y.; Wuttig, A.; Surendranath, Y. Mesostructure-Induced Selectivity in CO2 Reduction Catalysis. *J. Am. Chem. Soc.* **2015**, *137*, 14834−14837.

(5) Luc, W.; Collins, C.; Wang, S.; Xin, H.; He, K.; Kang, Y.; Jiao, F. Ag−Sn Bimetallic Catalyst with a Core−Shell Structure for CO2 Reduction. *J. Am. Chem. Soc.* **2017**, *139*, 1885−1893.

(6) Ulissi, Z. W.; Tang, M. T.; Xiao, J.; Liu, X.; Torelli, D. A.; Karamad, M.; Cummins, K.; Hahn, C.; Lewis, N. S.; Jaramillo, T. F.; Chan, K.; Nørskov, J. K. Machine-Learning Methods Enable Exhaustive Searches for Active Bimetallic Facets and Reveal Active Site Motifs for CO2 Reduction. *ACS Catal.* **2017**, *7*, 6600−6608.

(7) Humphrey, J. J. L.; Plana, D.; Celorrio, V.; Sadasivan, S.; Tooze, R. P.; Rodríguez, P.; Fermín, D. J. Electrochemical Reduction of Carbon Dioxide at Gold-Palladium Core-Shell Nanoparticles: Product Distribution versus Shell Thickness. *ChemCatChem* **2016**, *8*, 952−960.

(8) Clark, E. L.; Hahn, C.; Jaramillo, T. F.; Bell, A. T. Electrochemical CO2 Reduction over Compressively Strained CuAg Surface Alloys with Enhanced Multi-Carbon Oxygenate Selectivity. *J. Am. Chem. Soc.* **2017**, *139*, 15848−15857.

(9) Shinagawa, T.; Larrazábal, G. O.; Martín, A. J.; Krumeich, F.; Pérez-Ramírez, J. Sulfur-Modified Copper Catalysts for the Electrochemical Reduction of Carbon Dioxide to Formate. *ACS Catal.* **2018**, *8*, 837−844.

(10) Sun, K.; Cheng, T.; Wu, L.; Hu, Y.; Zhou, J.; Maclennan, A.; Jiang, Z.; Gao, Y.; Goddard, W. A.; Wang, Z. Ultrahigh Mass Activity for Carbon Dioxide Reduction Enabled by Gold-Iron Core-Shell Nanoparticles. *J. Am. Chem. Soc.* **2017**, *139*, 15608−15611.

(11) Hatsukade, T.; Kuhl, K. P.; Cave, E. R.; Abram, D. N.; Feaster, J. T.; Jongerius, A. L.; Hahn, C.; Jaramillo, T. F. Carbon Dioxide Electroreduction Using a Silver−Zinc Alloy. *Energy Technol.* **2017**, *5*, 955−961.

(12) Nesbitt, N. T.; Ma, M.; Trześniewski, B. J.; Jaszewski, S.; Tafti, F.; Burns, M. J.; Smith, W. A.; Naughton, M. J. Au Dendrite Electrocatalysts for CO2 Electrolysis. *J. Phys. Chem. C* **2018**, *122*, 10006−10016.

(13) Yoo, C. J.; Jae Dong, W.; Yong Park, J.; Wook Lim, J.; Kim, S.; Soon Choi, K.; Okello Odongo Ngome, F.; Choi, S.-Y.; Lee, J.-L. Compositional and Geometrical Effects of Bimetallic Cu−Sn Catalysts on Selective Electrochemical CO2 Reduction to CO. *ACS Appl. Energy Mater.* **2020**, *3*, 4466−4473.

(14) Christophe, J.; Doneux, T.; Buess-Herman, C. Electroreduction of Carbon Dioxide on Copper-Based Electrodes: Activity of Copper Single Crystals and Copper-Gold Alloys. *Electrocatalysis* **2012**, *3*, 139−146.

(15) Huang, Y.; Handoko, A. D.; Hirunsit, P.; Yeo, B. S. Electrochemical Reduction of CO2 Using Copper Single-Crystal Surfaces: Effects of CO* Coverage on the Selective Formation of Ethylene. *ACS Catal.* **2017**, *7*, 1749−1756.

(16) Sargeant, E.; Kolodziej, A.; Le Duff, C. S.; Rodriguez, P. Electrochemical Conversion of CO2 and CH4 at Subzero Temperatures. *ACS Catal.* **2020**, *10*, 7464−7474.

(17) Li, J.; Kuang, Y.; Meng, Y.; Tian, X.; Hung, W.-H.; Zhang, X.; Li, A.; Xu, M.; Zhou, W.; Ku, C.-S.; Chiang, C.-Y.; Zhu, G.; Guo, J.; Sun, X.; Dai, H. Electroreduction of CO2 to Formate on a Copper-Based Electrocatalyst at High Pressures with High Energy Conversion Efficiency. *J. Am. Chem. Soc.* **2020**, *142*, 7276−7282.

(18) Wuttig, A.; Surendranath, Y. Impurity Ion Complexation Enhances Carbon Dioxide Reduction Catalysis. *ACS Catal.* **2015**, *5*, 4479−4484.

(19) Li, X.; Gunathunge, C. M.; Agrawal, N.; Montalvo-Castro, H.; Jin, J.; Janik, M. J.; Waegele, M. M. Impact of Alkali Metal Cations and Iron Impurities on the Evolution of Hydrogen on Cu Electrodes in Alkaline Electrolytes. *J. Electrochem. Soc.* **2020**, *167*, No. 106505.

(20) Leung, K. Y.; McCrory, C. C. L. Effect and Prevention of Trace Ag+ Contamination from Ag/AgCl Reference Electrodes on CO2 Reduction Product Distributions at Polycrystalline Copper Electrodes. *ACS Appl. Energy Mater.* **2019**, *2*, 8283−8293.

(21) Luc, W.; Hee Ko, B.; Kattel, S.; Li, S.; Su, D.; G. Chen, J.; Jiao, F. SO2-Induced Selectivity Change in CO2 Electroreduction. *J. Am. Chem. Soc.* **2019**, *141*, 9902−9909.

(22) Varela, A. S.; Ju, W.; Reier, T.; Strasser, P. Tuning the Catalytic Activity and Selectivity of Cu for CO2 Electroreduction in the Presence of Halides. *ACS Catal.* **2016**, *6*, 2136−2144.

(23) Ovalle, V. J.; Waegele, M. M. Impact of Electrolyte Anions on the Adsorption of CO on Cu Electrodes. *J. Phys. Chem. C* **2020**, *124*, 14713−14721.

(24) Quan, F.; Xiong, M.; Jia, F.; Zhang, L. Efficient Electroreduction of CO2 on Bulk Silver Electrode in Aqueous Solution via the Inhibition of Hydrogen Evolution. *Appl. Surf. Sci.* **2017**, *399*, 48−54.

(25) Banerjee, S.; Han, X.; Thoi, V. S. Modulating the Electrode-Electrolyte Interface with Cationic Surfactants in Carbon Dioxide Reduction. *ACS Catal.* **2019**, *9*, 5631−5637.

(26) Garg, S.; Li, M.; Rufford, T. E.; Ge, L.; Rudolph, V.; Knibbe, R.; Konarova, M.; Wang, G. G. X. Catalyst−Electrolyte Interactions in Aqueous Reline Solutions for Highly Selective Electrochemical CO2 Reduction. *ChemSusChem* **2020**, *13*, 304−311.

(27) Seifitokaldani, A.; Gabardo, C. M.; Burdyny, T.; Dinh, C.-T.; Edwards, J. P.; Kibria, M. G.; Bushuyev, O. S.; Kelley, S. O.; Sinton, D.; Sargent, E. H. Hydronium-Induced Switching between CO 2 Electroreduction Pathways. *J. Am. Chem. Soc.* **2018**, *140*, 3833−3837.

(28) Waegele, M. M.; Gunathunge, C. M.; Li, J.; Li, X. How Cations Affect the Electric Double Layer and the Rates and Selectivity of Electrocatalytic Processes. *J. Chem. Phys.* **2019**, *151*, No. 160902.

(29) Strmcnik, D.; Kodama, K.; van der Vliet, D.; Greeley, J.; Stamenkovic, V. R.; Marković, N. M. The Role of Non-Covalent Interactions in Electrocatalytic Fuel-Cell Reactions on Platinum. *Nat. Chem.* **2009**, *1*, 466−472.

(30) Murata, A.; Hori, Y. Product Selectivity Affected by Cationic Species in Electrochemical Reduction of CO $_2$ and CO at a Cu Electrode. *Bull. Chem. Soc. Jpn.* **1991**, *64*, 123−127.

(31) Resasco, J.; Chen, L. D.; Clark, E.; Tsai, C.; Hahn, C.; Jaramillo, T. F.; Chan, K.; Bell, A. T. Promoter Effects of Alkali Metal Cations on the Electrochemical Reduction of Carbon Dioxide. *J. Am. Chem. Soc.* **2017**, *139*, 11277−11287.

(32) Singh, M. R.; Kwon, Y.; Lum, Y.; Ager, J. W.; Bell, A. T. Hydrolysis of Electrolyte Cations Enhances the Electrochemical Reduction of CO2 over Ag and Cu. *J. Am. Chem. Soc.* **2016**, *138*, 13006−13012.

(33) Ayemoba, O.; Cuesta, A. Spectroscopic Evidence of Size-Dependent Buffering of Interfacial PH by Cation Hydrolysis during

https://dx.doi.org/10.1021/acscatal.0c02387
ACS Catal. 2020, 10, 9907−9914

CO2 Electroreduction. *ACS Appl. Mater. Interfaces* **2017**, *9*, 27377−27382.
(34) Singh, M. R.; Clark, E. L.; Bell, A. T. Effects of Electrolyte, Catalyst, and Membrane Composition and Operating Conditions on the Performance of Solar-Driven Electrochemical Reduction of Carbon Dioxide. *Phys. Chem. Chem. Phys.* **2015**, *17*, 18924−18936.
(35) Chen, L. D.; Urushihara, M.; Chan, K.; Nørskov, J. K. Electric Field Effects in Electrochemical CO2 Reduction. *ACS Catal.* **2016**, *6*, 7133−7139.
(36) Zhao, S. F.; Horne, M.; Bond, A. M.; Zhang, J. Is the Imidazolium Cation a Unique Promoter for Electrocatalytic Reduction of Carbon Dioxide? *J. Phys. Chem. C* **2016**, *120*, 23989−24001.
(37) Kumeda, T.; Tajiri, H.; Sakata, O.; Hoshi, N.; Nakamura, M. Effect of Hydrophobic Cations on the Oxygen Reduction Reaction on Single−crystal Platinum Electrodes. *Nat. Commun.* **2018**, *9*, No. 4378.
(38) Atifi, A.; Boyce, D. W.; DiMeglio, J. L.; Rosenthal, J. Directing the Outcome of CO 2 Reduction at Bismuth Cathodes Using Varied Ionic Liquid Promoters. *ACS Catal.* **2018**, *8*, 2857−2863.
(39) Asadi, M.; Kim, K.; Liu, C.; Addepalli, A. V.; Abbasi, P.; Yasaei, P.; Phillips, P.; Behranginia, A.; Cerrato, J. M.; Haasch, R.; Zapol, P.; Kumar, B.; Klie, R. F.; Abiade, J.; Curtiss, L. A.; Salehi-Khojin, A. Nanostructured Transition Metal Dichalcogenide Electrocatalysts for CO2 Reduction in Ionic Liquid. *Science* **2016**, *353*, 467−470.
(40) Hollingsworth, N.; Taylor, S. F. R.; Galante, M. T.; Jacquemin, J.; Longo, C.; Holt, K. B.; De Leeuw, N. H.; Hardacre, C. Reduction of Carbon Dioxide to Formate at Low Overpotential Using a Superbase Ionic Liquid. *Angew. Chem., Int. Ed.* **2015**, *54*, 14164−14168.
(41) Feaster, J. T.; Jongerius, A. L.; Liu, X.; Urushihara, M.; Nitopi, S. A.; Hahn, C.; Chan, K.; Nørskov, J. K.; Jaramillo, T. F. Understanding the Influence of [EMIM]Cl on the Suppression of the Hydrogen Evolution Reaction on Transition Metal Electrodes. *Langmuir* **2017**, *33*, 9464−9471.
(42) Sarkar, S.; Maitra, A.; Banerjee, S.; Sara Thoi, V.; M. Dawlaty, J. Electric Fields at Metal−Surfactant Interfaces: A Combined Vibrational Spectroscopy and Capacitance Study. *J. Phys. Chem. B* **2020**, *124*, 1311−1321.
(43) Zhang, Z.-Q.; Banerjee, S.; Thoi, V. S.; Shoji Hall, A. Reorganization of Interfacial Water by an Amphiphilic Cationic Surfactant Promotes CO 2 Reduction. *J. Phys. Chem. Lett.* **2020**, *11*, 5457−5463.
(44) Murata, A.; Hori, Y. Product Selectivity Affected by Cationic Species in Electrochemical Reduction of CO2 and CO at a Cu Electrode. *Bull. Chem. Soc. Jpn.* **1991**, *64*, 123−127.
(45) Osawa, M.; Tsushima, M.; Mogami, H.; Samjeské, G.; Yamakata, A. Structure of Water at the Electrified Platinum−Water Interface: A Study by Surface-Enhanced Infrared Absorption Spectroscopy. *J. Phys. Chem. C* **2008**, *112*, 4248−4256.
(46) Ringe, S.; Clark, E. L.; Resasco, J.; Walton, A.; Seger, B.; Bell, A. T.; Chan, K. Understanding Cation Effects in Electrochemical CO2 Reduction. *Energy Environ. Sci.* **2019**, *12*, 3001−3014.
(47) Gunathunge, C. M.; Ovalle, V. J.; Waegele, M. M. Probing Promoting Effects of Alkali Cations on the Reduction of CO at the Aqueous Electrolyte/Copper Interface. *Phys. Chem. Chem. Phys.* **2017**, *19*, 30166−30172.
(48) Mandal, A. B.; Unni Nair, B. Cyclic Voltammetric Technique for the Determination of the Critical Micelle Concentration of Surfactants, Self-Diffusion Coefficient of Micelles, and Partition Coefficient of an Electrochemical Probe. *J. Phys. Chem. A* **1991**, *95*, 9008−9013.
(49) Paria, S.; Khilar, K. C. A Review on Experimental Studies of Surfactant Adsorption at the Hydrophilic Solid-Water Interface. *Adv. Colloid Interface Sci.* **2004**, *110*, 75−95.
(50) Manne, S.; Cleveland, J. P.; Gaub, H. E.; Stucky, G. D.; Hansma, P. K. Direct Visualization of Surfactant Hemimicelles by Force Microscopy of the Electrical Double Layer. *Langmuir* **1994**, *10*, 4409−4413.
(51) Li, J.; Li, X.; Gunathunge, C. M.; Waegele, M. M. Hydrogen Bonding Steers the Product Selectivity of Electrocatalytic CO Reduction. *Proc. Natl. Acad. Sci. U.S.A.* **2019**, *116*, 9220−9229.
(52) Pérez-Gallent, E.; Marcandalli, G.; Figueiredo, M. C.; Calle-Vallejo, F.; Koper, M. T. M. Structure- and Potential-Dependent Cation Effects on CO Reduction at Copper Single-Crystal Electrodes. *J. Am. Chem. Soc.* **2017**, *139*, 16412−16419.

https://dx.doi.org/10.1021/acscatal.0c02387
ACS Catal. 2020, 10, 9907−9914